minerals

MDPI

Article

Mono and Poly-Cationic Adsorption of Heavy Metals Using Natural Glauconite

Małgorzata Franus [1,*], Lidia Bandura [2,*] and Jarosław Madej [2]

1 Department of Construction, Faculty of Civil Engineering and Architecture, Lublin University of Technology, Nadbystrzycka 40, 20-618 Lublin, Poland
2 Department of Geotechnical Engineering, Faculty of Civil Engineering and Architecture, Lublin University of Technology, Nadbystrzycka 40, 20-618 Lublin, Poland
* Correspondence: m.franus@pollub.pl (M.F.); l.bandura@pollub.pl (L.B.); Tel.: +48-81-5384428 (M.F.); +48-81-5384451 (L.B.)

Received: 28 May 2019; Accepted: 28 July 2019; Published: 31 July 2019

Abstract: The issue of heavy metal pollution of industrial wastewaters is a major environmental concern nowadays. The aim of this study was to investigate the effectiveness of heavy metals removal from aqueous solutions by natural glauconite, in batch and dynamic systems. Glauconite was characterized by X-ray diffraction, nitrogen adsorption–desorption isotherm, scanning electron microscope, differential thermal analysis, and inductively coupled plasma spectroscopy. Cation exchange capacity, bulk density and point of zero charge were also determined. In the batch system, the impact of initial concentration, contact time, and pH of metal solutions on sorption efficiency was analysed, whereas for the dynamic system, the influence of flow rate was studied. The adsorption capacity in the batch system followed the order: Pb > Cd > Zn > Cu. The highest adsorption rate was achieved in the pH range 7–9. In the column experiments, the selectivity order in the case of mono-cationic system was the same as that of batch system, whereas in the case of poly-cationic system it was: Pb > Zn > Cd > Cu. With the increase of the flow rate, the total capacity at the exhaustion point increased.

Keywords: glauconite; heavy metals; adsorption; batch system; fixed-bed column

1. Introduction

Heavy metals belong to the group of most dangerous pollutants and exhibit a negative impact on human health and ecosystems [1]. Their harmful effect is related to their ability to accumulate in tissues of living organisms, which causes numerous disorders. Heavy metals constitute common components of wastes from industry sectors, including electroplating, metal finishing, metallurgical, tannery, chemical manufacturing, mining, and battery manufacturing [2]. Insufficient treatment of municipal, industrial, and agricultural wastewaters leads to the discharging of heavy metals into the environment, in developing countries [3].

The most commonly found heavy metals in municipal waters are cadmium (Cd), lead (Pb), zinc (Zn), and copper (Cu) [4,5]. Cadmium accumulated in the human body can cause erythrocyte destruction, nausea, drooling, diarrhea, muscle cramps, kidney disease, chronic lung problems, and skeleton deformations. Zinc is a trace element responsible for the physiological functions of tissues and regulating many biochemical processes. However, too much zinc might be responsible for health problems, such as stomach cramps, skin irritation, vomiting, nausea, or anemia [6]. The main source of zinc in wastewaters is the non-ferrous metal industry, textile industry, chemical, and electrochemical industries. Copper is a component needed for the growth of living organisms, but in excessive amount it can cause various diseases in the pancreas, liver, skin, brain and heart muscles [7], or cause vomiting

and cramps [8]. Lead is an element that naturally occurs in the mineral form. The emission of dangerous forms of lead to the environment occurs as a result of human activity, especially metallurgy and glasswork, oil and rubber industry, pesticide production, outdated printers, battery production, fuel combustion, and other automotive pollution. Lead ions exhibit the ability to bind to some enzymes and interfere with the central nervous system, impairs the function of hematopoietic, reproductive, renal, and hepatic systems [9].

Many different methods for purification of wastewaters from heavy metals were proposed like, ion exchange [10], electrochemical separation [11], precipitation [12], coagulation–flocculation [13], flotation [14], membrane processes [15], and adsorption [16]. Among them, the adsorption method is considered to be very effective in terms of environmental and economic factors [17]. Adsorption techniques are recommended for the removal of heavy metals, at their low concentrations, from aqueous media. To this aim various adsorbents have been applied, including polymeric resins, zeolites, minerals, activated carbon, or novel advanced materials [18–21]. However, using natural clay minerals seems to be a simple and efficient solution for hydrometallurgy and wastewater treatment technologies. Clay minerals are natural, locally available, commonly occurring, and low-cost adsorbents [22]. The adsorption method, although a well-known and effective process, is rarely used on an industrial scale due to the high costs of adsorbents, which is disproportionate to the economic effects of purification. However, finding a low-cost and easy available natural material might change this situation.

Glauconite is rich in iron-layered silicate type 2:1. It occurs in the sedimentary rocks of all geological ages, in contemporary oceanic sediments in the vicinity of continents, and in islands on shelves, continental slopes, and oceanic heights. Its form of occurrence makes this mineral concentrate cheap and profitable to obtain. Specific morphology, internal structure and chemical composition of glauconite provide this mineral with specific surface area, ion exchange capacity, and catalytic properties that determine its application. So far, glauconite has been used for the removal of radionuclides [23], lead, zinc, and cadmium ions in static conditions [24]. As a source of potassium, it is applied as a slow-release fertilizer with high content of magnesium, iron, and biomicroelements [25], and as a mineral for rock-dating [26].

The aim of this study was to study the performance of Polish glauconite from the Lublin region in the purification of aqueous solutions containing heavy metal ions, in batch and fixed-bed column adsorption systems. Different batch variables were examined, including a contact time, initial concentration, and pH. In case of the fixed-bed column study, the influence of flow rate was examined and the Thomas model was applied to predict the breakthrough curves for ion exchange. After the sorption process, the glauconite could be re-used as a sustainable and environment-friendly building material, as reported by Franus et al. 2011 [27].

2. Materials and Methods

2.1. Materials

Glauconite of the Lublin region occurs in tertiary sediments of quartz sands and muds associated with Upper Paleogene sedimentation (Eocene and Oligocene). The petrographic form of these sediments allows for easy and economically justified extraction of glauconite using magnetic separation. The glauconite was magnetically separated from quartz sand using a neodymium-samarium magnet. A fraction of 125–500 µm was selected for the study.

The glauconite chemical characterization was performed by ICP atomic emission spectroscopy (Thermo Jarrell Ash Corporation, Franklin, TN, USA). The SiO_2, Al_2O_3, Fe_2O_3, MnO, MgO, CaO, Na_2O, K_2O, P_2O_5, Ba, Sr, Sc, Zr, V, and Y were analyzed using 0.2 g of the sample melted with lithium metaborate and dissolved in 15% HNO_3. Other elements were analyzed by the plasma-induced mass spectrometry method on an ICP/MS spectrometer (Elan 6000, Perkin Elmer, Wellesley, MA, USA). For this purpose, 0.2 g of the sample was melted with a mixture of lithium metaborate and lithium tetraborate in an induction furnace, and then dissolved in 5% HNO_3.

The glauconite cation exchange capacity was determined using a method recommended by the international organization AIPEA (International Association for the Study of Clay) [28], on the basis of the amount of Ba^{2+} ions in the saturated sample, which was desorbed with 1 M $MgCl_2$. Bulk density was determined on the basis of the Polish Standard PN-80-C-04532-Determination of bulk density. Point of zero charge for glauconite was determined using the potentiometric titration method.

Textural parameters of glauconite (specific surface area S_{BET}, surface, volume and diameter of pores) were determined using nitrogen adsorption/desorption isotherms measured at the temperature of liquid nitrogen, using ASAP 2020MP, manufactured by Micromeritics (Norcross, GA, USA).

Differential thermal analysis was performed using the Derivatograph C System (Paulik-Paulik-Erdey, Budapest, Hungary). A sample of 0.3 g was tested in an air atmosphere at a temperature range of 20–1000 °C. Al_2O_3 was used as the thermally inert substance. The temperature ramping rate was 10 °C/min. The result of the measurement was the differential thermal curve (DTA curve) and the sample loss curve (TG curve).

The mineral composition of glauconite was determined by X-ray diffraction (XRD) using X'pert PROMPD spectrometer (Panalytical, Almelo, The Netherlands) with a PW 3050/60 goniometer (Panalytical), a Cu lamp, and a graphite monochromator. The analysis was performed within the angle range of 5°–65° (2 Theta). Philips X'Pert Highscore software (High Score Plus v. 4.1, Panalytical, Almelo, The Netherlands) was used to process the diffraction data. The identification of mineral phases was based on the PDF-2 release 2010 database formalized by the ICDD (The International Centre for Diffraction Data). The morphology was determined by means of a scanning electron microscope (SEM) FEI Quanta 250 FEG (FEI, Hilsboro, OR, USA).

2.2. Batch Adsorption Experiments

Heavy metal ions removal was determined in terms of—the initial concentration, pH, and the contact time. A stock solution of each metal was prepared by dissolving an appropriate amount of $Pb(NO_3)_2$, $Zn(NO_3)_2{\cdot}6H_2O$, $Cd(NO_3)_2{\cdot}3H_2O$, and $Cu(NO_3)_2{\cdot}3H_2O$ (Merc), in distilled water. A given amount of glauconite samples were placed in the conical flasks, which were filled with the metal solutions of the given volume and concentrations. The suspensions were shaken at 25 °C at 150 rpm for a specified time and then centrifuged at 10,000 rpm for 10 min. The concentration of metals in the solutions, before and after adsorption, was determined using the atomic absorption spectroscopy (AAS) performed on the Philips PU-9100X spectrometer (Philips, Almelo, The Netherlands). The pH of the stock solutions was modified with the use of 0.1 M HCl and 0.1 M NaOH and measured with pHmeter (Orbeco-Hellige, Sarasota, FL, USA).

For studying the influence of the initial metal concentration, 1.0 ± 0.01 g of the glauconite sample and 100 mL of heavy metal solution in the concentration range (C_0) 5–220 mg/L and pH 4.0 were used. The suspensions were shaken for 24 h.

In the study of the impact of the contact time, 4.5 g of the glauconite sample, 450 mL of the stock solutions of heavy metal ions of C_0 = 50 mg/L and pH 4.0 were used. The suspensions were shaken for different intervals of time ranging from 5 to 2880 min and then centrifuged.

The influence of pH was studied using 0.5 g of glauconite sample, 40 mL of heavy metal solutions in the pH range of 3–10 and C_0 = 50 mg/L. The shaking time was 24 h.

The amount of metals removed from the solution was calculated from the difference in metal ion concentrations in solution, before and after the adsorption process, according to the formula:

$$Q = \frac{(C_0 - C_{eq}) \cdot V}{W} \tag{1}$$

where Q—amount of metal ions removed by 1 mass unit of glauconite, (mg/g), C_0—initial concentration of heavy metal in the solution, (mg/L), C_{eq}—heavy metal concentration in solution after ion exchange process, (mg/L), V—solution volume, (L), and W—mass of the mineral, (g).

2.3. Fixed-Bed Column Experiments

Under dynamic conditions, heavy metals were removed from gravitationally flowing mono- and poly-cationic solutions. Glauconite sample (12 g) was placed in glass columns with a diameter of 1 cm and a length of 50 cm. After being poured from the top with deionized water, the samples formed beds of about 8 cm height. The constant level of the liquid height during the flow was maintained by a peristaltic pump. The metal concentrations in effluents were measured by absorption spectrometry (AAS) on a Philips P-9100X spectrometer (Philips, Almelo, The Netherlands). An illustration of the performed experiment is presented in Figure 1.

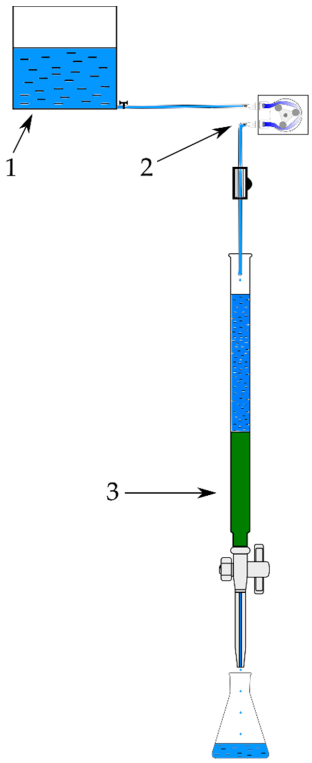

Figure 1. Schematic illustration of the fixed-bed column experiments. 1—heavy metal solution; 2—peristaltic pump; 3—glauconite bed.

The initial concentration of mono-cations were 46, 51, 52, and 49 mg/L for Cd, Cu, Zn, and Pb, respectively. Removal of heavy metal ions from the poly-cationic solutions was performed for variable linear flow velocity of solutions (v_1 = 1.22 mL/min, v_2 =1.66 mL/min, v_3 = 2.11 mL/min). The concentrations of metals in poly-cationic solution were: Pb(II)—20.18 mg/L, Cd(II)—11.05 mg/L, Zn(II)—6.98 mg/L, and Cu(II)—6.63 mg/L. The breakthrough point was determined when the concentration of the particular heavy metal was equal or below the recommended and permitted values according to the regulations (Regulation of the Minister of the Environment, Journal of Laws 137). The limits were as follows, for Zn(II)—2 mg/L, Pb(II), Cd(II) and Cu(II)—0.1 mg/L. The exhaustion time and the total capacity at the exhaustion point of the bed were assumed to be the concentration of heavy metal in the leakage that reached the initial concentration C_0 [29,30]. The total (equilibrium) capacity at the exhaustion point A_C was defined as the total amount of solute immobilized in the bed (or exchanged during the process of ion exchange in the fixed-bed of packed materials). It was determined by integration of the area above the S-curve up to the exhaustion point:

$$A_C = \frac{\int_0^{V_C}(C_0 - C)dV}{\rho HA} = \frac{\int_0^{V_C}(C_0 - C)dV}{m} \quad (2)$$

where C_0 is the initial concentration in mg/L, C is the effluent concentration in mg/g, V_c is the effluent volume at which the point of exhaustion of the bed occurs (absolute or normalized to the bed volume) in mL, ρ is the packing density of the bed in g/cm^3, H is the length of the bed in cm, A is the cross-section area of the bed in cm^2, m is the mass of the adsorbent in g.

The breakthrough capacity A_D of the bed could be calculated by the following expression:

$$A_D = \frac{\int_0^{V_D}(C_0 - C)dV}{\rho HA} = \frac{C_0 V_D}{m} \quad (3)$$

where V_D is the effluent volume collected up to the breakthrough point in cm^3.

3. Results and Discussion

3.1. Glauconite Characteristics

The investigated mineral was a popular type of glauconite that belonged to the dioctahedral mica group. The general crystallochemical formula could be represented as: $K_{0.83}[\left(R^{3+}_{1.33}R^{2+}_{0.67}\right)(Al_{0.13}Si_{3.87}O_{10}(OH)_2]$. The chemical analysis of glauconite indicated that the main components were SiO_2 (50.52%); Fe_2O_3 (20.17%), K_2O (8.40%), Al_2O_3 (6.04%), and MgO (4.2%). The trace amounts were, chromium—206 ppm, rubidium—250 ppm, vanadium—148 ppm, zinc—79 ppm, and zirconium—55 ppm. The high potassium content suggested that the illite packets dominated the glauconite structure. On the other hand, the low content of CaO (0.42%) and Na_2O (0.07%) suggested small amounts of swelling packages in the studied clay that could be confirmed by the XRD analysis (Figure 2).

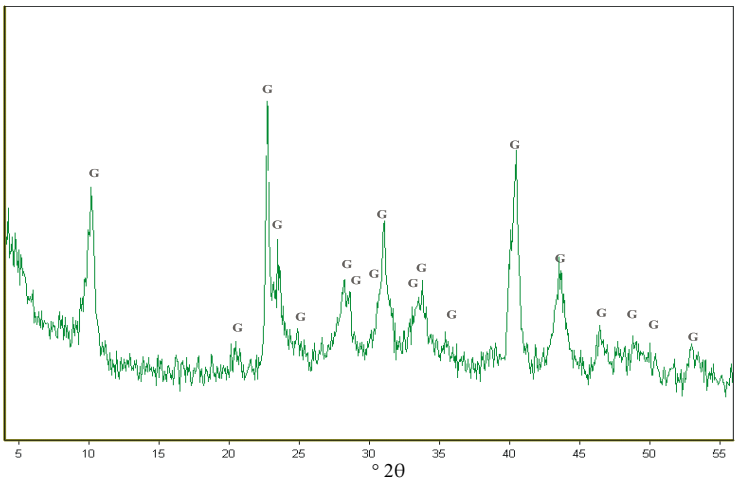

Figure 2. XRD patterns of glauconite.

The presence of the glauconite mineral phases was determined by interplanar d-values d_{hkl}: 10.07; 4.55, 3.65; 3.33; 3.1; 2.586; 2.401; 2.256; and 2.154 Å. On the X-ray diffraction patterns, the main diffraction reflections characteristic of this material were clearly visible. Glauconite represented the ordered structure with the order type ISII and the swelling packets content between 5% and 15%, which could be classified as a politype 1 M. This politype meant that the glauconite had a well-ordered structure, contained small contribution of swelling packets, and possessed a high content of K_2O (potassium is the main exchangeable cation). Table 1 presents the physicochemical parameters of glauconite, among which specific surface area (S_{BET}), cation exchange capacity (CEC), and point of zero charge (pH_{pzc}) were most responsible for the heavy metals adsorption processes.

Table 1. Physico-chemical parameters of glauconite.

Parameter	Value
S_{BET} (m^2/g)	78.44
V_{mic} (cm^3/g)	0.005
S_{mes} (m^2/g)	67.21
V_{mes} (cm^3/g)	0.086
CEC (meq/100 g)	17
Bulk density (g/cm^3)	1.38
Point of zero charge, pH_{pzc}	6.48

S_{BET}—specific surface area, V_{mic}—micropore volume, V_{mes}—mesopore volume, CEC—cation exchange capacity.

The DTA/TG thermal analysis revealed a clear endothermic effect associated with the presence of molecular water at a temperature range of 100 to 200 °C, with a maximum temperature at 145 °C (Figure 3). The other two endothermic effects were weak—one with a maximum at 525 °C, associated with dehydroxylation; the loss of OH^+ groups, and the second at 920 °C—related to the breakdown of the crystalline glauconite network. The total mass loss reached 9.5%. Two last, weak, and blurred thermal effects might be attributed to the young geological age (tertiary period) and ordered crystallographic structure of the glauconite, which has been confirmed by radiometric studies [26].

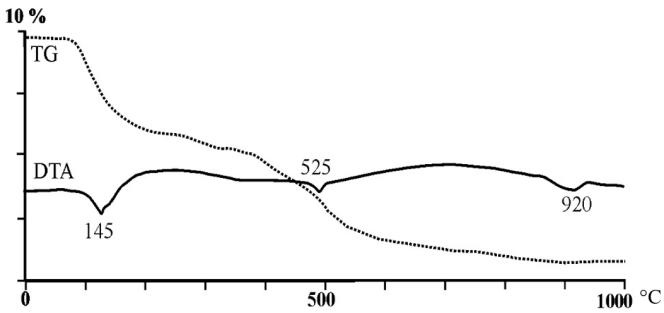

Figure 3. Curves of thermal differential analysis (differential thermal curve (DTA)/sample loss curve (TG)) of glauconite.

SEM images of the glauconite are presented in Figure 4. It created spherical, loaf-shaped, ellipsoidal aggregates called pellets. Most of them were smooth, often cracked, and sometimes filled with secondary materials like ferric oxides.

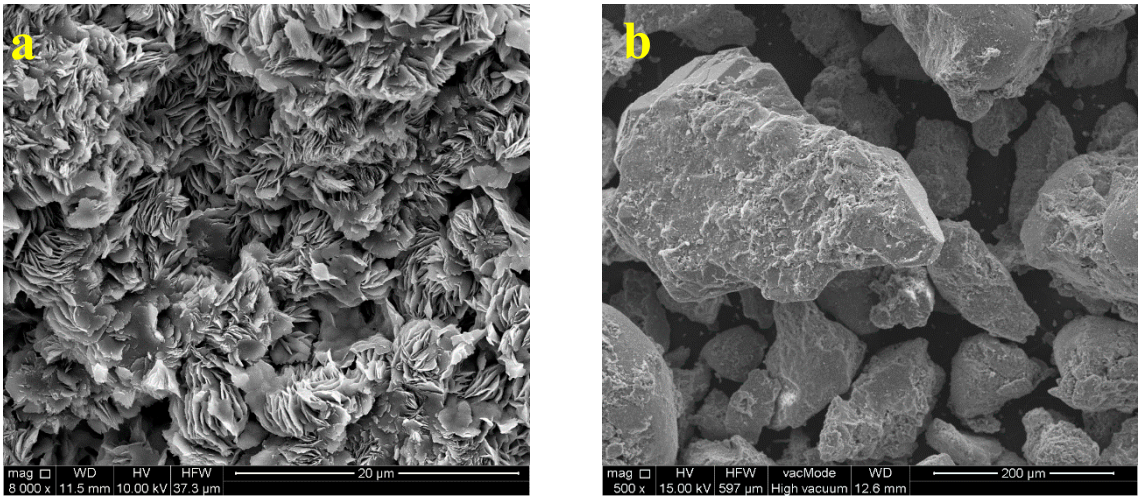

Figure 4. SEM image of glauconite—shell-shaped, 8000× magnification (**a**) and aggregates of round shape, 200× magnification (**b**).

3.2. Batch Experiments

3.2.1. Effect of Contact Time

By studying the kinetics of metal adsorption from aqueous solutions on glauconite, the time required to obtain the equilibrium concentration (ionic equilibrium state) was determined. The resulting values of adsorption capacity and removal efficiency for individual metal ions are shown in Table 2.

Table 2. Adsorption capacities (q_t) and removal efficiencies (E) of heavy metal ions on glauconite.

Time (min)	Zn		Cd		Cu		Pb	
	q_t (mg/g)	E (%)	q_t (mg/g)	E (%)	q_t (mg/g)	E (%)	q_t (mg/g)	E (%)
5	1.174	22.91	1.422	27.87	1.363	27.04	1.968	40.78
10	1.478	28.82	1.855	36.24	1.567	31.03	2.497	51.33
20	1.573	30.66	2.001	39.20	1.748	34.65	2.694	55.39
40	1.795	34.96	2.254	44.14	1.935	38.38	3.222	66.13
80	1.906	37.17	2.428	47.48	2.104	41.69	3.553	73.07
180	1.980	38.60	2.523	49.40	2.218	43.98	3.753	77.07
360	1.975	38.53	2.596	50.76	2.291	45.40	3.875	79.64
720	2.018	39.34	2.602	50.94	2.301	45.20	3.895	79.96
1440	2.040	39.77	2.602	50.92	2.266	44.91	3.885	79.85
2880	2.027	39.50	2.625	51.37	2.237	44.32	3.916	80.41

Within the first five minutes of the contact time, 41% of the total Pb(II), 28%—Cd(II), Cu(II)—27%, and 23% Zn(II) was immobilized by glauconite. The time required to reach the ionic equilibrium was about 360 min for Cu(II), Cd(II), Pb(II), and for Zn(II)—180 min. The amount of adsorbed ions at equilibrium were as follows—1.98 mg/g for zinc, 2.291 mg/g for copper, 2.596 mg/g for cadmium, and 3.875 mg/g for lead ions. After this, the adsorption capacity was maintained at a constant level indicating a total saturation of the active sites of the material. Glauconite exhibited the highest adsorption capacity with respect to Pb(II), followed by Cd(II), then Cu(II), and Zn(II). The greater the adsorption capacity, the higher was the removal efficiency. Removal efficiency in the equilibrium was the highest for the Pb(II) ions and the lowest for the Zn(II).

The kinetics of adsorption described the rate of adsorbate uptake on adsorbent and it controlled the equilibrium time [29]. The kinetics parameters were used to determine the adsorption rate necessary for the design and modeling of the removal processes [30]. In order to analyze the rate of heavy metal adsorption on glauconite, pseudo-first-order (PFO), pseudo-second-order (PSO), and intraparticle diffusion models (IPD) were used [31,32]. In the pseudo-first-order kinetics model, the reaction rate was directly proportional to the difference in the equilibrium adsorbate concentration and the temporary concentration in the solid phases:

$$\frac{dq_t}{dt} = k_1(q - q_t) \tag{4}$$

The pseudo-second-order kinetics model assumes the proportionality of process rate proportional to the square of the difference in the adsorbate equilibrium concentration and temporary concentration in the adsorbent solid phase:

$$\frac{dq_t}{dt} = k_2(q - q_t)^2 \tag{5}$$

After the integration and ordering of the equation, they take the following linear form:

- pseudo-first-order model,

$$log(q - q_t) = log(q) - kt \tag{6}$$

- pseudo-second-order model,

$$\frac{t}{q_t} = \frac{1}{k_2 q^2} + \frac{1}{q} \tag{7}$$

Linear regression of the above relationships allows to estimate the model value of the adsorbate concentration on the adsorbent surface and the constant saturation rate of the sorbent capacity (k_1 and k_2). If the outlined curves lay in a straight line, then the confirmation of the order of saturation process of the deposit (first or second) was obtained. Linear regression of both models allowed to determine, both, the metal ion concentration values on the sorbent surface and the process rate values (k_1, k_2).

The Weber and Morris model, known as intraparticle diffusion, assumes that adsorption varies linearly with the square of the contact time. It is expressed by the following equation:

$$q_t = K_{id} \cdot t^{0.5} + D \tag{8}$$

where, K_{id} is the rate constant of intraparticle diffusion (mg/(g·min$^{0.5}$)), $t^{0.5}$ is the square root of the time, and D is the intercept related to the thickness of the boundary layer.

When the plot q_t vs. $t^{0.5}$ is linear and passes through the origin, the main rate-limiting step for the adsorption is intraparticle diffusion process. On the other hand, if the relationship q_t vs. $t^{0.5}$ does not pass through the origin or is non-linear, the adsorption process is accompanied by other mechanisms [33].

Figure 5 shows the kinetic plots for the three examined models and Table 3 presents the kinetic parameters determined from the PFO, PSO, and the IPD equations. The PFO equation could not be applied to interpret the adsorption kinetics due to the low quality of fitting to the experimental data and the consequent large deviations from linearity, especially near the equilibrium state. The PSO equation fitted very well to the experimental data, evidenced by high correlation coefficients close to 1 (Table 3), as well as similar values of adsorption capacity to the experimental values. Therefore, it was more likely that the adsorption behaviour might involve valence forces through electrons sharing between the metal ions and the adsorbent [34]. The velocity constant k_2 determined from the PSO model had the greatest value for Cu(II) and the lowest value for the Pb(II) ions.

Table 3. Kinetic parameters for the adsorption of heavy metals on glauconite.

Parameter		Zn	Cd	Cu	Pb
C_0		51.3	51.1	50.4	48.7
q_e		2.04	2.62	2.30	3.92
PFO	q_c (mg/g)	0.37	0.36	0.71	0.62
	k_1 (min^{-1})	0.004	0.003	0.012	0.003
	R^2	0.753	0.619	0.985	0.626
PSO	q_c (mg/g)	2.03	2.63	2.25	3.92
	k_2 (g/mg·min)	0.100	0.061	2.251	0.035
	R^2	1.000	1.000	0.999	1.000
IPD	K_{ida}	0.0031	0.0024	0.0034	0.0022
	D_a (mg/g)	0.033	0.023	0.038	0.016
	R^2	0.887	0.878	0.949	0.943
	K_{idb}	5.18×10^{-5}	3.30×10^{-5}	6.25×10^{-5}	2.93×10^{-5}
	D_b (mg/g)	0.060	0.045	0.069	0.036
	R^2	0.875	0.594	0.905	0.578

C_0—the initial concentration, q_e—experimental equilibrium sorption capacity, PFO—pseudo-first-order model, PSO—pseudo-second-order model, IPD—intraparticle diffusion model, q_c—equilibrium sorption capacity calculated from PFO/PSO, k_1—rate constant for PFO, k_2—rate constant for PSO, K_{ida}/K_{idb}—intraparticle diffusion rate constants in area a or b, and D_a/D_b—Weber and Morris constant proportional to the boundary layer thickness in area a or b.

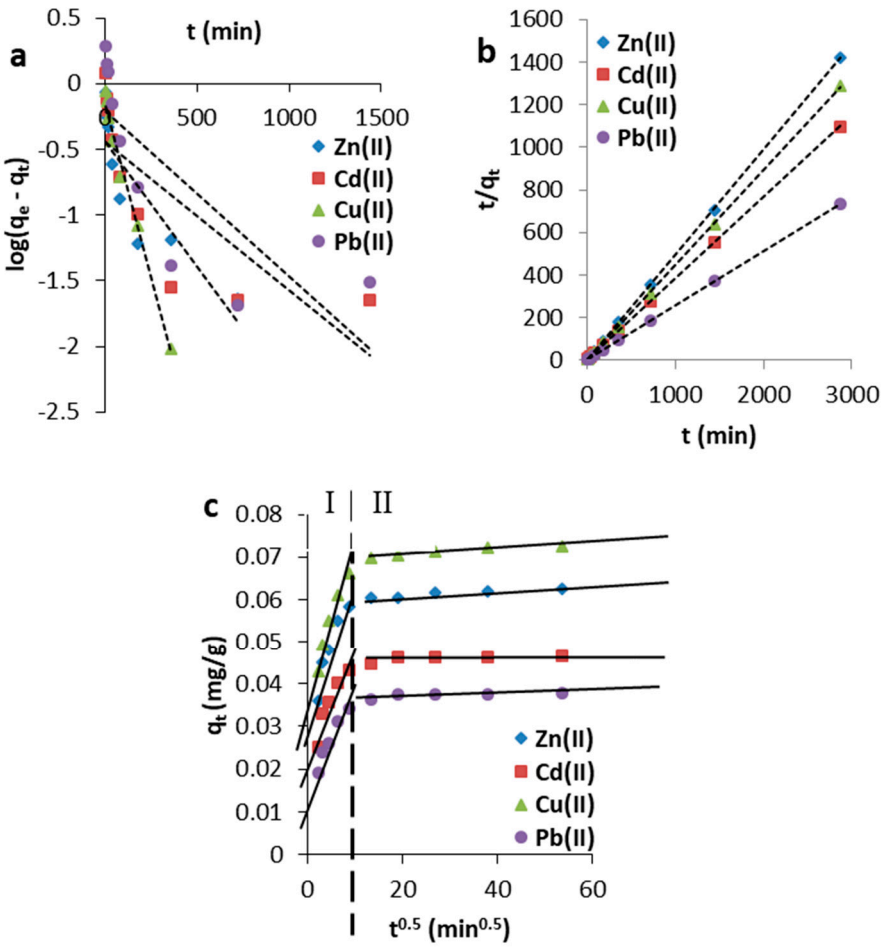

Figure 5. The kinetic plots of (**a**) pseudo-first-order (PFO), (**b**) pseudo-second-order (PSO), (**c**) intraparticle diffusion (IPD) models for heavy metal adsorption on glauconite.

Intraparticle diffusion was not the sole rate-limiting step (the plots q_t vs. $t^{0.5}$ do not pass through the origin). As shown in Figure 5c the adsorption involved two steps: (a) the initial step (I) represented by the steep linear plot, which might be associated with surface diffusion (external surface adsorption); and a second step (II) represented by the less steep plot, which might be assigned to the very slow adsorption of adsorbates in the equilibrium state. The slope of the line at stages (a) and (b) was denoted as the rate parameters K_{ida} and K_{idb}, respectively (Table 3). The adsorption rate K_{ida} was much higher than K_{idb} for each metal. The resistance to the external mass transfer increased as the intercept (constant D) increased [35]. The constant D was higher for the second stage of adsorption, indicating an increase of the boundary layer and a decrease of external mass transfer, which simultaneously might be attributed to the increase of internal mass transfer. Lowest values of D for Pb ions reflected their lowest resistance to the external mass transfer.

3.2.2. Effect of Initial Concentration

The effect of initial concentration on the adsorption of Pb(II), Cu(II), Zn(II), and Cd(II) metal ions was studied at concentrations 5, 10, 20, 50, 100, and 220 mg/L. Under equilibrium conditions, the amount of a substance adsorbed by the adsorbent could be determined by the equation:

$$\frac{X}{M} = \frac{(C_0 - C_e)\cdot V}{M} \tag{9}$$

where X/M (typically expressed as mg pollutant/g media) is mass of pollutant per mass of media, C_0 is the initial concentration in solution (mg/L), C_e is the equilibrium concentration (mg/L), V is the volume of the solution to which the media mass is exposed (L), and M is the mass of the media (g).

Adsorption isotherms are presented in Figure 6. The amount of adsorbed metals increased with an increase in the initial adsorbate concentration from 5 to 50 mg/L. At lower concentrations the ratio of the number of heavy metal ions to the number of available adsorption sites was relatively small. The process of adsorption was independent of the initial concentration, but with the increase of heavy metals ions/glauconite ratio, exchangeable sites became saturated, which caused a decrease in the adsorption efficiency [36].

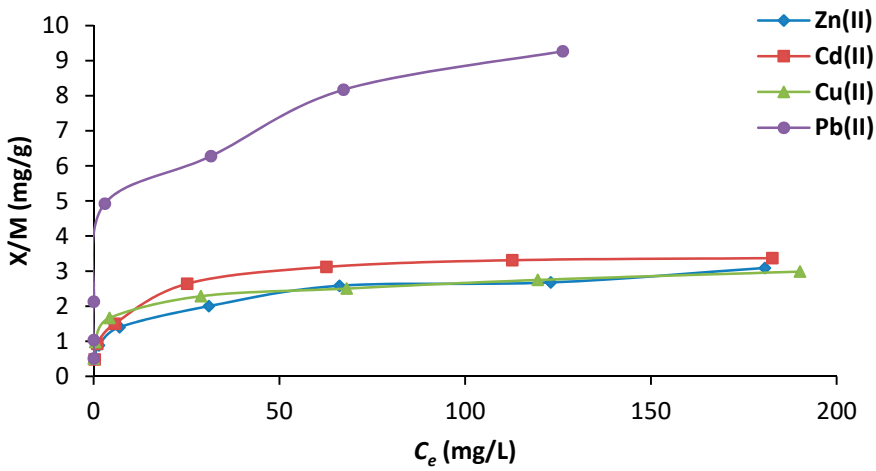

Figure 6. Adsorption isotherms of heavy metals for glauconite.

The compatibility of the adsorption results with the Freundlich, Langmuir, and Temkin adsorption isotherms was tested. The Langmuir adsorption isotherm has been successfully applied to many adsorption processes and has been the most widely used adsorption isotherm model applied to aqueous media [37,38]. The Langmuir isotherm is based on the assumption that adsorption occurs at specific active sites of identical energy on the surface of the adsorbent, without significant interaction between the adsorbate molecules, which form a monolayer on the adsorbent surface.

The general Langmuir model is defined by the equation:

$$\frac{X}{M} = \frac{(K_L - C_e)}{1 + a_L \cdot C_e} \tag{10}$$

where X/M is the amount of solute retained per unit weight of the sorbent (mg/g), C_e is equilibrium concentration of solute remaining in the solution (mg/L), K_L (L/mg), and a_L (mg/g) are the isotherm constants that can be determined using linear regression. K_L is related to the energy of adsorption and a_L is the maximum adsorption capacity. The higher the K_L value, the stronger the bond between the metal ion and the mineral surface.

The essential characteristics of the Langmuir isotherm could be characterized by a separation factor or equilibrium constant K_R [39], which is defined as:

$$K_R = \frac{1}{1 + K_L \cdot C_0} \tag{11}$$

where K_R is a dimensionless separation factor, C_0 is the initial concentration (mg/L), and K_L is the Langmuir constant (L/mg).

The parameter K_R indicates the shape of the isotherm, accordingly, $K_R > 1$-unfavorable, $K_R = 1$-linear, $0 < K_R <$/1-favourable, and $K_R = 0$-irreversible.

The Freundlich model could be applied to the non-ideal systems, including multilayer adsorption processes on heterogeneous surfaces. The Freundlich adsorption isotherm equation was as follows:

$$\frac{X}{M} = K_F(C_e)^{1/n} \tag{12}$$

where, K_F [mg/g·(L/mg)1/n] and n are adsorption capacity and affinity, respectively, determined from the linear plot of lnX/M vs. logC_e.

The Freundlich constant K_f expressed the adsorbent capacity and n was the heterogeneity factor. For favourable adsorption n value ranged between 0 and 1 (and 1/n should be in the range of 1–10).

The Temkin model [40] took into account the effects of indirect adsorbate–adsorbate interactions on adsorption isotherms, and assumed that the heat of adsorption would more often decrease than increase with increasing coverage. The equation is as follows:

$$\frac{X}{M} = \frac{RT}{b} \cdot \ln(T_i \cdot C_e) \tag{13}$$

where T is the absolute temperature (K), R is the gas constant, T_i is the Temkin isotherm constant (L/g), b is the Temkin constant related to the heat of adsorption (kJ/mol), and C_e is the equilibrium concentration (mg/L). The parameters T_i and b and the correlation coefficient R^2 can be determined by the linear regression from the relationship X/M versus lnC_e.

The linear plots of the adsorption isotherms as well as isotherm constants, together with the correlation coefficients (R^2) from the linear regressions are presented in Figure 7 and Table 4, respectively.

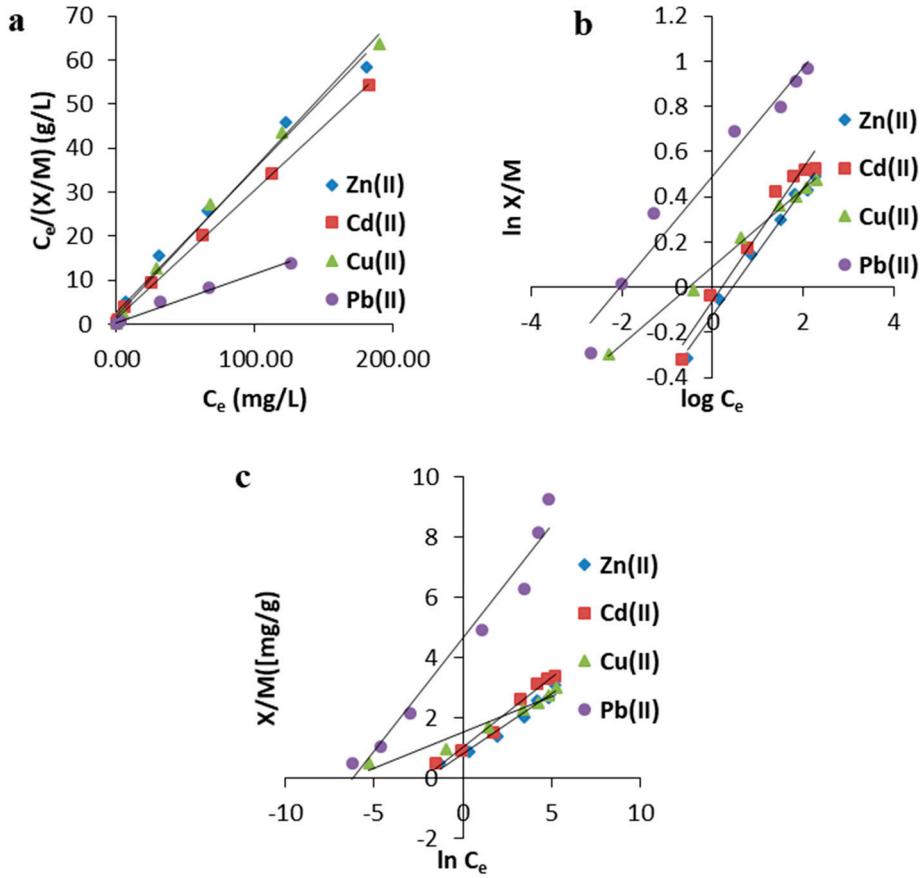

Figure 7. The linear plots of (**a**) Langmuir, (**b**) Freundlich, and (**c**) Temkin isotherms for heavy metal ion adsorption on glauconite.

Table 4. Values of isotherm constants for metal ions adsorption onto glauconite.

Isotherm Model	Parameter	Zn	Cd	Cu	Pb
Langmuir	a_L (mg/g)	3.072	3.438	2.960	9.099
	K_L (L/mg)	0.117	0.206	0.210	0.310
	R^2	0.988	0.999	0.994	0.986
Freundlich	K_F (mg/g(L/mg)$^{1/n}$)	0.758	0.870	1.231	3.103
	$1/n$	3.596	3.420	5.831	4.137
	R^2	0.989	0.973	0.996	0.963
Temkin	b (kJ/mol)	6.237	5.309	10.353	3.277
	K_T (L/g)	7.835	9.146	560.442	463.249
	R^2	0.973	0.978	0.952	0.963

Analysis of the correlation coefficient R^2 suggested that the Langmuir model was the best at describing the adsorption equilibrium. The monolayer saturation capacities, a_L, followed the order, Pb > Cd > Zn > Cu and corresponded well with the adsorption capacities determined experimentally. However, taking into account the R^2, the Freundlich and Temkin models also fit the sorption of heavy metal ions. Adsorption on a heterogeneous surface might be considered since glauconite as a raw mineral might exhibit heterogenic surface. The values of $1/n$ suggested a favourable adsorption. A value of the constant b determined from the Temkin isotherm model for Pb was the lowest, which could be attributed to the highest degree of surface coverage. A strong relationship between b (degree of coverage) and the adsorption capacity could be observed, where a higher b value corresponded to a smaller sorption capacity.

The K_R values (Figure 8) indicated that adsorption was more favorable for higher initial metal concentrations. Adsorption was the most favourable for lead ions and least for Zn. In contrast, K_R for Cd and Cu was at a very similar level. According to this classification, the favorability system tended to be in the order, Pb > Cu > Cd > Zn.

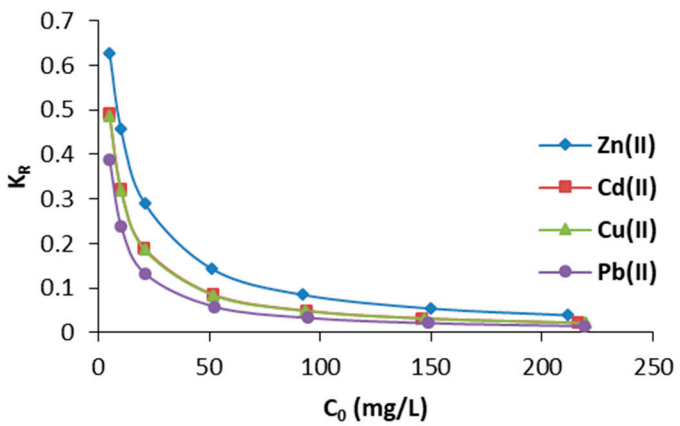

Figure 8. Plots of separation factor K_R against the initial metal concentration.

3.2.3. Effect of pH

The solution pH had a significant impact on the heavy metals capture, as it determined the adsorbent surface charge, ionization degree, and adsorbate speciation. Changes in pH caused that the adsorption processes that coexisted with the precipitation of hydroxides. Typically, the adsorption of cations increases with the increase of pH from zero to almost 100% [41]. The gradual increase in pH lead to (a) the formation of complex ions; and (b) precipitation of metal ions in the form of hydroxides. The decrease of heavy metal ions in the solution was the result of the adsorption process

of cations on the glauconite surface. The adsorption was accompanied by the formation of complexes $MeOH^+$ and the precipitation of hydroxides $Me(OH)_2$, at higher pH values [42]. Theoretical hydroxide precipitation pH using the values of the solubility product K_{sp} was estimated for each metal. Figure 9 shows the removal efficiency of the heavy metals as a function of pH at a heavy metal concentration of 50 mg/L and a glauconite concentration of 20 g/L. In general, the E(%) increased as the pH increased, and sharply reached over 90% at a specific pH value.

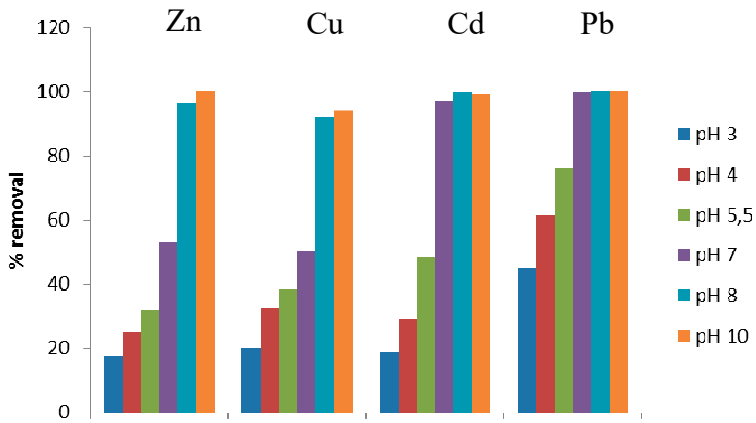

Figure 9. Effect of pH on the adsorption of heavy metals by glauconite.

Lead sorption processes were dominant at the pH range 3.0–5.5. In this range E(%) increased from 45.16% to 76%, respectively. At pH 7, more than 99% of lead ions were removed from the solution. It was connected with the negatively charged surface of the glauconite, when pH of the equilibrium solution was higher than pH_{pzc}. In a higher pH, a significant amount of lead hydroxide might begin to precipitate.

The precipitation pH was also theoretically calculated (pH about 6), according to the maximum concentration of lead and its constant solubility product ($K_{sp} = 1.43 \times 10^{-20}$).

Zinc was predominantly adsorbed at the pH range 3–7. With a further pH increase up to 8.0, zinc removal efficiency increased to 98.8% and at pH above 8.0 to almost 100%. In all probability, significant amounts of zinc hydroxide were precipitated at pH 7.1, which meant that zinc ions were removed from the solution by hydrolysis ($K_{sp} = 1.2 \times 10^{-17}$).

In the case of copper removal efficiency at a pH of 3.0 to 5.5, about 18.88% to 48.52% of the ions were removed. The pH increase up to 7 led to the immobilization of 97% of the copper ions. In all probability, a significant amount of copper hydroxide $Cu(OH)_2$ was precipitated at around pH 5.7, which was determined on the basis of the constant solubility product ($K_{sp} = 2.2 \times 10^{-20}$).

In the pH range from 3 to 7, glauconite removed about 20.18% to 50.31% of the cadmium from the aqueous solution. The increase in pH to 8 resulted in a rapid removal of Cd(II) ions from the solution (92%). As pH > pH_{pzc}, the surface of glauconite became negatively charged. The increase in pH up to 10 resulted in a complete immobilization of cadmium ions (100%). At higher pH, a hydrolysis reaction might occur, causing a precipitation of Cd(II) in the form of hydroxides. The theoretical pH value for cadmium hydroxide precipitation was above 8 and could be calculated on the basis of the solubility product $K_{sp} = 7.2 \times 10^{-15}$.

In general, the removal efficiency was the highest above the pH_{pzc} of glauconite.

3.3. Column Studies

According to Volesky [43], three factors determine the shape and slope of the breakthrough curve, the equilibrium adsorption relationships, the mass transfer to and throughout the bed, and operation parameters. In the dynamic systems the solution flows continuously through packed particles of the adsorbent, which makes the sorption process different from that of a batch system. Since kinetics

in beds is influenced by diffusion rates in the material and the whole equilibrium curve, sorption results obtained in the fixed bed systems are more representative than those obtained in batch systems. In practice, the knowledge about the influence of each operational parameter on the adsorption system is of great importance and constitutes a valuable engineering tool [44].

To predict the relationship between the concentration and time in column studies, the Thomas model was applied. It assumes that adsorption is controlled by mass transfer rather than chemical interactions. The model is suitable for describing the breakthrough curves and estimating the maximum adsorption capacity [45].

The Thomas equation is as follows:

$$\frac{C}{C_0} = \frac{1}{1 + \exp\left(\frac{k_{Th} Q_0 M}{F} - k_{Th} C_0 t\right)} \tag{14}$$

where k_{Th} is the Thomas model constant (L/mg·min), Q_0 is the maximum solid-phase concentration of solute (mg/g), M is the sorbent amount (g), F is the flow rate (L/min). Thomas model parameters could be determined from the plot of $\ln(C_0/C - 1)$ versus t at a given flow rate; k_{Th} from slope of the plot, and Q_0 from intercept of the plot.

The breakthrough curves for the heavy metal ions removal from mono-cationic and poly-cationic aqueous solutions are presented in Figures 10 and 11, respectively. The experimental results are plotted as C/C_0 versus time, where C is the metal ion effluent concentration (mg/L) and C_0 is the metal ion initial concentration (mg/L). The breakthrough curves exhibited a similar shape for each metal.

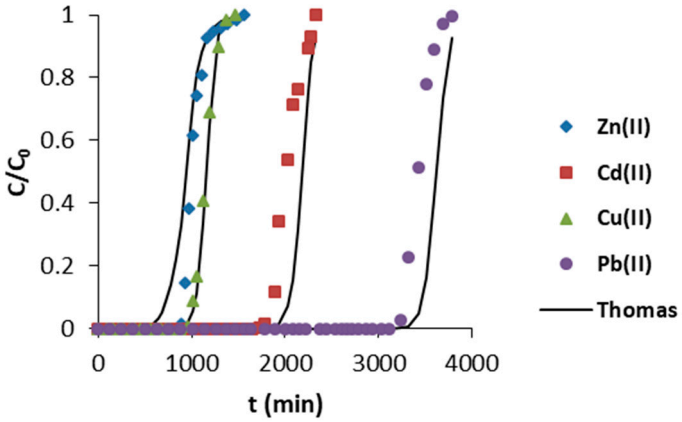

Figure 10. Breakthrough curves of Zn, Cu, Cd, and Pb adsorption from mono-cationic solutions.

The breakthrough curve parameters for the removal of Pb(II), Cu(II), Zn(II), and Cd(II) from the mono-cationic solutions are summarized in Table 5. The breakthrough time for the removal of Cu(II) was the shortest and led to purify 890 mL of the solution. After 1045 min—1130 mL of zinc ions was removed. In similar time (1083 min) 1520 mL of cadmium solution was purified. The longest breakthrough time (3403 min) and the highest capacity at the exhaustion point (12.527 mg/g) was noted for the removal of Pb(II). After reaching the breakthrough point, a gradual increase of the metal ion concentration in the effluent and saturation of the glauconite sorption complex occurred. Exhaustion of the ion exchange properties of the material was achieved after pouring of 1520 mL of Cu(II), 1650 mL of Zn(II), 2190 mL of Cd(II), and 3510 mL of Pb(II) through the bed. The Thomas model provided a good fit to the experimental data with R^2 in the range of 0.909–0.983. The breakthrough time, experimental total capacity of the bed A_c and Q_0 determined from the Thomas model revealed the following order, Pb(II) > Cd(II) > Zn(II) > Cu(II) towards examined heavy metal ions, however, theoretical Q_0 values were slightly higher than the experimental bed capacities (Table 5).

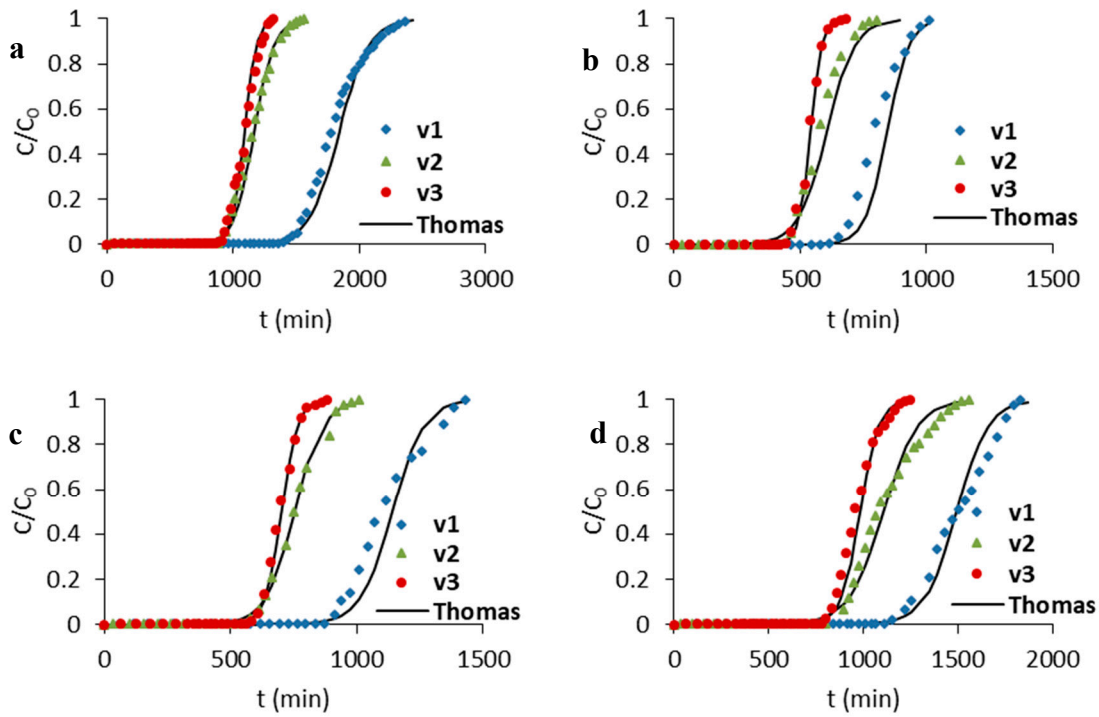

Figure 11. Breakthrough curves of (**a**) Zn, (**b**) Cd, (**c**) Cu, and (**d**) Pb on glauconite at different flow rates (v_1 = 1.35, v_2 = 1.78, and v_3 = 2.23 cm^3/min).

Table 5. Parameters of heavy metal removal from mono-cationic metal solutions by glauconite and the Thomas model parameters (m = 12 g, bed depth-8 cm, V = 1 mL/min).

Parameter	Zn	Cd	Cu	Pb
C_0 (mg/L)	52	46	51	49
t_D(min)	1045	1083	788	3403
t_C (min)	1565	2330	1465	3790
V_D (mL)	1130	1520	890	2770
V_C (mL)	1650	2190	1520	3510
A_D (mg/g)	4.680	5.252	3.357	11.310
A_C (mg/g)	5.359	6.999	4.741	12.527
k_{Th} (L/mg·min)	0.000210	0.000373	0.000386	0.000309
Q_0 (mg/g)	5.211	7.854	5.099	13.755
R^2	0.909	0.960	0.981	0.954

C_0—initial concentration, (mg/L), V_D—breakthrough volume, (cm^3); V_C—exhaustion volume, (mL); t_D—breakthrough time, (min); t_C—exhaustion time, (min); A_D—total capacity at the breakthrough point, (mg/g); A_C—total capacity at the exhaustion point, (mg/g); k_{Th}—Thomas model constant, (L/mg·min); Q_0—maximum solid-phase concentration of solute, (mg/g); and R^2—correlation coefficient.

In the case of metal removal from poly-cationic solution (Figure 11), with an increase in the flow rates of the ion exchange capacity, breakthrough time and the exhaustion time of the bed decreased. Table 6 presents the breakthrough curve parameters of the heavy metals removal from poly-cationic solution by glauconite, at various flow rates. As the flow rate of zinc solution increased from 1.35 to 2.23 mL/min, the breakthrough time and the exhaustion time decreased from 1690 to 1315 min and from 2426 min to 1315 min, respectively.

Table 6. Parameters of the fixed-bed glauconite (mixed metals solutions) and the Thomas model parameters (m = 12 g, v_1 = 1.35 mL/min, v_2 = 1.78 mL/min, and v_3 = 2.23 mL/min).

Parameter	Zn			Cd			Cu			Pb		
C_0 (mg/L)	6.98			11.05			6.63			20.18		
	v_1	v_2	v_3	v_1	v_2	v_3	v_1	v_2	v_3	v_1	v_2	v_3
t_D (min)	1690	1070	1035	673	447	450	895	570	590	1120	820	790
t_C (min)	2426	1560	1315	1067	890	680	1428	1010	882	1870	1558	1248
V_D (BV) (cm^3)	1900	1650	2080	725	760	880	1040	1005	1200	1390	1450	1660
V_C (BV) (cm^3)	2850	2470	2710	1310	1570	1410	895	570	590	1120	820	790
A_d, (mg/g)	0.8	08	088	1.46	1.4	1.57	1.12	1.06	1.28	4.406	4.608	5.314
A_C (mg/g)	1.21	1.20	1.30	1.49	1.44	1.58	1.63	1.73	1.74	6.27	6.52	6.94
k_{Th} (L/mg min·10^{-3})	1.212	1.821	2.960	2.120	1.60	4.130	2.419	2.648	4.782	0.596	0.548	0.995
Q_0 (mg/g)	1.446	1.210	1.415	1.049	0.992	1.110	0.849	0.740	0.864	3.384	3.309	3.682
R^2	0.955	0.964	0.950	0.966	0.627	0.969	0.772	0.983	0.980	0.907	0.899	0.928

V_D—breakthrough volume, (cm^3); V_C—exhaustion volume, (mL); t_D—breakthrough time, (min); t_C—exhaustion time, (min); A_d—capacity at the breakthrough point, (mg/g); A_C—total capacity at the exhaustion point, (mg/g); k_{Th}—Thomas model constant, k_{Th} (L/mg·min); Q_0—maximum solid-phase concentration of solute, (mg/g); and R^2—correlation coefficient.

The exhaustion time of the bed for Zn(II) decreased 1.8 times. A similar tendency could be noted for the rest metals for which the breakthrough time and the exhaustion time decreased from 1.41 to 1.61, within the increase of the flow rate. At a lower flow rate, the adsorbate residence time was longer thus, enhancing the adsorbate–adsorbent interactions. The higher flow rate slightly increased the capacity at the breakthrough point of the bed. For example, the capacity at the breakthrough point towards Pb(II) at v_1, v_2, and v_3 was 4.36, 4.78, and 5.54 mg/g, respectively, and a similar trend could be observed towards the rest of metals. By increasing the flow rate, the solute did not have enough time to achieve an adsorption equilibrium, so the heavy metals solutions left the bed before establishing an equilibrium state in the adsorption complex [46,47]. On the other hand, using low flow rates prolonged the processing time, which is not desirable in practice, taking into account that large volumes of wastewaters have to be purified [29].

The Thomas model fit well to the experimental data with R^2 in the range of 0.907 to 0.983 for almost all metals. Only in the case of Cd(II) removal at v_2 and Cu(II) at v_1, the correlation coefficients were lower, 0.627 and 0.772, respectively, showing a deviation from the Thomas model's theoretical assumptions. The experimental bed capacity and Q_0 in the case of heavy metals removal at different flow rates followed the order: Pb > Zn > Cd > Cu. The selectivity order revealed that Zn(II) was removed more efficiently than Cd(II) in the case of the poly-cationic solutions, whereas for the mono-cationic solution, Cd(II) exhibited a higher A_d and A_c, and thus, was removed more efficiently. In all probability, it was related to the similar ionic radii of both metals ($h_{r\mathrm{Zn}}$ = 4.30 Å, $h_{r\mathrm{Cd}}$ = 4.26 Å). Additionally, no concurrent interactions occurred in the mono-cationic system which could affect the removal efficiency. Hydrated ionic radii (h_r) of the metals led to predict their selectivity order, which was usually inversely proportional to h_r, and reflected their favorability to be introduced into interlayers and bind with planar sites of the clay.

4. Conclusions

In the batch system, glauconite revealed the highest sorption capacity towards Pb(II) ions, followed by Cd(II), Zn(II), and Cu(II). Within the increase in concentration of solutions, the amount of heavy metals removed increased until the mineral active sites were saturated. The time needed to reach the ionic equilibrium was about 360 min for Cu(II), Cd(II), Pb(II), and was much shorter for Zn(II)—180 min. The amount of adsorbed ions at the, equilibrium state was as follows for zinc 1.98 mg/g, for copper 2.291 mg/g, for cadmium 2.596 mg/g, and for lead ions 3.875 mg/g. The higher pH of heavy metal solutions enhanced adsorption efficiency. In the pH range from 3 to 7, adsorption was the only

mechanism of heavy metals immobilization, while precipitation of metal hydroxides took place above pH = 7.

The glauconite effectively removed the Pb, Cd, Zn, and Cu in the dynamic system. In the mono-cationic systems, at the breakthrough point, the order of preference of the glauconite for metal ions in terms of milligrams of metal removed per gram of mineral was, Pb > Cd > Zn > Cu. In the case of equal par ions, the hydrodynamic radius was the most important aspect. With the increase of atomic mass of heavy metal ions, their hydrodynamic radius decreased. It meant that their interchangeable energy increased the energy input to glauconite. Lead ions have the highest molecular weight, and therefore, have a particular connection to the structure of glauconite.

In poly-cationic systems, the order of preference of the glauconite for metal ions in terms of milligrams of metal removed per gram of mineral was, Pb > Zn > Cd > Cu.

The breakthrough curve for adsorption in a column packed with glauconite demonstrated that lead ions adsorb preferentially in comparison to other metals. The increase in flow rates slightly influenced the capacity at the breakthrough and the total capacity at the exhaustion point, towards higher values. Studied glauconite, occurring in the Tertiary quartz-glauconite sediments of the Lublin Upland, proved to be an effective mineral for the removal of heavy metals, in batch and column studies. The dynamic column system might constitute a basis to design a treatment system to separate and recover metals from metal bearing wastewaters.

Author Contributions: Conceptualization, M.F.; methodology, M.F., L.B., and J.M.; investigation, M.F. and L.B.; resources, M.F.; data curation, M.F., L.B., and J.M.; writing—original draft preparation, M.F. and L.B.; writing—review and editing, J.M.

Funding: This work was supported by the statutory funds No. FN12/ILT/2019.

Acknowledgments: Lidia Bandura was supported by the Foundation for Polish Science (FNP).

Conflicts of Interest: The authors declare no conflict of interest. The funders had no role in the design of the study; in the collection, analyses, or interpretation of data; in the writing of the manuscript, or in the decision to publish the results.

References

1. Bove, D.; Merello, S.; Frumento, D.; Al Arni, S.; Aliakbarian, B.; Converti, A. A critical review of biological processes and technologies for landfill leachate treatment. *Chem. Eng. Technol.* **2015**, *38*, 2115–2126. [CrossRef]
2. Ayari, F.; Srasra, E.; Trabelsi-Ayadi, M. Retention of lead from an aqueous solution by use of bentonite as adsorbent for reducing leaching from industrial effluents. *Desalination* **2007**, *206*, 270–278. [CrossRef]
3. Gupta, D.A. Implication of environmental flows in river basin management. *Phys. Chem. Earth.* **2008**, *33*, 298–303. [CrossRef]
4. Kyzioł-Komosińska, J.; Rosik-Dulewska, C.; Franus, M.; Antoszczyszyn-Szpicka, P.; Czupioł, J.; Krzyżewska, I. Sorption Capacities of Natural and Synthetic Zeolites for Cu(II) Ions. *Pol. J. Environ. Stud.* **2015**, *24*, 1111–1123. [CrossRef]
5. Demirbas, A. Heavy metal adsorption onto agro-based waste materials: A review. *J. Hazard. Mater.* **2008**, *157*, 220–229. [CrossRef] [PubMed]
6. Oyaro, N.; Juddy, O.; Murago, E.N.M.; Gitonga, E. The contents of Pb, Cu, Zn and Cd in meat in Nairobi, Kenya. *Int. J. Food Agric. Environ.* **2007**, *5*, 119–121.
7. Wang, S.; Terdkiatburana, T.; Tad'e, M.O. Adsorption of Cu(II), Pb(II) and humic acid on natural zeolite tuff in single and binary systems. *Sep. Purif. Technol.* **2008**, *62*, 64–70. [CrossRef]
8. Paulino, A.T.; Minasse, F.A.S.; Guilherme, M.R.; Reis, A.V.; Muniz, E.C.; Nozaki, J. Novel adsorbent based on silkworm chrysalides for removal of heavy metals from wastewaters. *J. Colloid Interface Sci.* **2006**, *301*, 479–487. [CrossRef]
9. Naseem, R.; Tahir, S.S. Removal of Pb(II) from aqueous solution by using bentonite as an adsorbent. *Water Res.* **2001**, *35*, 3982–3986. [CrossRef]
10. Hamdaoui, O. Removal of copper(II) from aqueous phase by purolite C100-MB cation exchange resin in fixed bed columns: modeling. *J. Hazard. Mater.* **2009**, *161*, 737–746. [CrossRef]

11. Akbal, F.; Camcı, S. Copper, chromium and nickel removal from metal plating wastewater by electrocoagulation. *Desalination* **2011**, *269*, 214–222. [CrossRef]
12. Mirbagheri, S.A.; Hosseini, S.N. Pilot plant investigation on petrochemical wastewater treatment for the removal of copper and chromium with the objective of reuse. *Desalination* **2005**, *171*, 85–93. [CrossRef]
13. Shammas, N.K. Coagulation and flocculation. In *Physicochemical Treatment Processes*, 3rd ed.; Wang, L.K., Hung, Y.-T., Shammas, N.K., Eds.; Humana Press: Clifton, NJ, USA, 2004; pp. 103–140.
14. Wang, L.K.; Fahey, E.M.; Wu, Z.C. Dissolved air flotation. In *Physicochemical Treatment Processes*, 3rd ed.; Wang, L.K., Hung, Y.-T., Shammas, N.K., Eds.; Humana Press: Clifton, NJ, USA, 2004; pp. 431–500.
15. Kurniawan, T.A.; Chan, G.Y.S.; Lo, W.; Babel, S. Physico-chemical treatment techniques for wastewater laden with heavy metals. *Chem. Eng. J.* **2006**, *118*, 83–98. [CrossRef]
16. Rao, M.M.; Ramesh, A.; Rao, G.P.; Seshaiah, K. Removal of copper and cadmium from the aqueous solutions by activated carbon derived from Ceiba pentandra hulls. *J. Hazard. Mater.* **2006**, *129*, 123–129. [PubMed]
17. Zheng, Y.A.; Huang, D.J.; Wang, A.Q. Chitosan-g-poly(acrylic acid) hydrogel with crosslinked polymeric networks for Ni^{2+} Recovery. *Chim. Acta* **2011**, *687*, 193–200. [CrossRef] [PubMed]
18. Chen, Y.; Zhao, W.; Yang, X.; Li, Y. Efficient removal of heavy metal ions from aqueous solution by a novel poly (1-vinylimidazole) chelate resin. *Polym. Bull.* **2019**, *76*, 1081–1097. [CrossRef]
19. Luo, H.; Law, W.W.; Wu, Y.; Zhu, W.; Yang, E.H. Hydrothermal synthesis of needle-like nanocrystalline zeolites from metakaolin and their applications for efficient removal of organic pollutants and heavy metals. *Microporous Mesoporous Mater.* **2019**, *272*, 8–15. [CrossRef]
20. Li, Z.; Wu, L.; Sun, S.; Gao, J.; Zhang, H.; Zhang, Z.; Wang, Z. Disinfection and removal performance for Escherichia coli, toxic heavy metals and arsenic by wood vinegar-modified zeolite. *Ecotoxicol. Environ. Saf.* **2019**, *174*, 129–136. [CrossRef] [PubMed]
21. Eeshwarasinghe, D.; Loganathan, P.; Vigneswaran, S. Simultaneous removal of polycyclic aromatic hydrocarbons and heavy metals from water using granular activated carbon. *Chemosphere* **2019**, *223*, 616–627. [CrossRef] [PubMed]
22. Sis, H.; Uysal, T. Removal of heavy metal ions from aqueous medium using Kuluncak (Malatya) vermiculites and effect of precipitation on removal. *Appl. Clay Sci.* **2014**, *95*, 1–8. [CrossRef]
23. Stefanova, I.G. Natural sorbents as barriers against migration of radionuclides from radioactive waste repositories. *Nat. Mic. Mat. Environ. Tech.* **1999**, *362*, 370–379.
24. Hao, O.J.; Tsai, C.M. The removal of metals and ammonium by natural glauconite. *Environ. Int.* **1987**, *13*, 203–212. [CrossRef]
25. Griffioen, J. Potassioum adsorption ratios as an indicator for the fate of agricultural potassium in groundwater. *J. Hydrol.* **2001**, *254*, 244–254. [CrossRef]
26. Derkowski, A.; Środoń, J.; Franus, W.; Uhlik, P.; Banaś, M.; Zieliński, G.; Caplovicova, M.; Franus, M. Partial dissolution of glauconitic samples: implications for the methodology of K-Ar and Rb-Sr dating. *Clays Clay Miner.* **2009**, *57*, 531–554. [CrossRef]
27. Franus, W.; Franus, M.; Latosińska, J.; Wójcik, R. The use of spent glauconite in lightweight aggregate production. *Bol. Soc. Esp. Ceram V.* **2011**, *50*, 193–200. [CrossRef]
28. Gillman, G.P. A proposed method for measurement of exchange properties of highly weathered soils. *Aust. J. Soil. Res.* **1979**, *17*, 129–139. [CrossRef]
29. Chu, K.H. Improved fixed bed models for metal biosorption. *Chem. Eng. J.* **2004**, *97*, 233–239. [CrossRef]
30. Medvidović Vukojević, N.; Perić, J.; Trgo, M. Column performance in lead removal from aqueous solutions by fixed bed of natural zeolite—Clinoptilolite. *Sep. Purif. Technol.* **2006**, *49*, 237–244. [CrossRef]
31. Tassist, A.; Lounici, H.; Abdi, N.; Mameri, N. Equilibrium, kinetic an thermodynamic studies on aluminum biosorption by a mycelial biomas (Streptomeces rimosus). *J. Hazard. Mater.* **2010**, *183*, 35–43. [CrossRef] [PubMed]
32. Weber, W.J.; Morris, J.C. Equilibria and capacities for adsorption on carbon. *J. Sanit. Eng. Div.* **1964**, *90*, 79–108.
33. Moura, C.P.; Vidal, C.B.; Barros, A.L.; Costa, L.S.; Vasconellos, L.C.G.; Dias, F.S.; Nascimento, R.F. Adsorption of BTX (benzene, toluene, o-xylene, and p-xylene) from aqueous solutions by modified periodic mesoporous organosilica. *J. Colloid Interface Sci.* **2011**, *363*, 626–634. [CrossRef] [PubMed]

34. Chen, A.H.; Liu, S.C.; Chen, C.Y.; Chen, C.Y. Comparative adsorption of Cu(II), Zn(II), and Pb(II) ions in aqueous solution on the crosslinked chitosan with epichlorohydrin. *J. Hazard. Mater.* **2008**, *154*, 184–191. [CrossRef] [PubMed]
35. Alshameri, A.; Yan, C.; Al-Ani, Y.; Dawood, A.S.; Ibrahim, A.; Zhou, C.; Wang, H. An investigation into the adsorption removal of ammonium by salt activated Chinese (Hulaodu) natural zeolite: Kinetics, isotherms, and thermodynamics. *J. Taiwan Inst. Chem. Eng.* **2014**, *45*, 554–564. [CrossRef]
36. Mishra, P.C.; Patel, R.K. Removal of lead and zinc ions from water by low cost adsorbents. *J. Hazard. Mater.* **2009**, *168*, 319–325. [CrossRef] [PubMed]
37. Langmuir, I. The constitution and fundamental properties of solids and liquids. *J. Am. Chem. Soc.* **1916**, *38*, 2221–2295. [CrossRef]
38. Ho, Y.S.; Huang, C.T.; Huang, H.W. Equilibrium sorption isotherm for metal ions on tree fern. *Process Biochem.* **2002**, *37*, 1421–1430. [CrossRef]
39. Deepthi, R.R.; Sasidhar, P. Sorption of Cesium on Clay Colloids: Kinetic and Thermodynamic Studies. *Aquat. Chem.* **2012**, *18*, 281–296. [CrossRef]
40. Tempkin, M.; Pyzhev, V. Kinetics of ammonia synthesis on promoted iron catalysts. *Acta Physico-Chimica Sin USSR* **1940**, *12*, 327–356.
41. Davis, J.A.; Hayes, K.F. Geochemical processes at mineral surfaces: An overview. In *American Chemical Society Symposium Series 323*; American Chemical Society: Washington, DC, USA, 1986; pp. 2–18.
42. Smith, E.; Lu, W.; Vengris, T.; Binkiene, R. Sorption of heavy metals by Lithuanian glauconite. *Water Res.* **1996**, *30*, 2883–2892. [CrossRef]
43. Volesky, B. Biosorption process simulation tools. *Hydrometallurgy* **2003**, *71*, 179–190. [CrossRef]
44. Inglezakis, V.J.; Grigoropoulou, H. Effects of operating conditions on the removal of heavy metals by zeolite in fixed bed reactors. *J. Hazard. Mater.* **2004**, *B112*, 37–43. [CrossRef] [PubMed]
45. Husein, D.Z.; Al-Radadi, T.; Danish, E.Y. Adsorption of phosphate using alginate-/zirconium-grafted newspaper pellets: fixed-bed column study and application. *J. Sci. Eng.* **2017**, *42*, 1399–1412. [CrossRef]
46. Aguayo-Villarreal, I.A.; Bonilla-Petriciolet, A.; Hernández-Montoya, V.; Montes–Morán, M.A.; Reynel-Avila, H.E. Batch and column studies of Zn^{2+} removal from aqueous solution using chicken feathers as sorbents. *Chem. Eng. J.* **2011**, *167*, 67–76. [CrossRef]
47. Ramirez, A.; Giraldo, S.; Garcia-Nunez, J.; Florez, E.; Acelas, N. Phosphate removal from water using a hybrid material in a fixed-bed column. *J. Water Process Eng.* **2018**, *26*, 131–137. [CrossRef]